# Method of Moment Analysis of Wire Antennas

Alex D. Santiago-Vargas
*Electrical and Computer Engineering*
*Purdue University*
West Lafayette, IN
adsv@purdue.edu

***Abstract*—The Method of Moments is a numerical technique that calculates surface currents and finds the induced fields in all space. Wire antennas are represented by line segments and can be solved quickly using this technique. This report presents the MoM implementation to calculate the input impedance, surface current, and antenna directivity for a series of dipoles. The impedance convergence is shown for increasing mesh discretization and compared to the analytical solution. The radiation pattern is calculated from the resulting current distribution.**

***Index Terms*—Method of Moments, Wire Antennas, Dipole**

## I. Introduction

Wire antennas are widely used for their simplicity, low cost, and versatility. Heinrich Hertz first demonstrated radio waves using dipoles, a linear wire antenna with a length of $\lambda/2$ at the frequency of operation [1]. Hertz also used a loop antenna as a receiver, which is a circular wire loop. Guglielmo Marconi continued by pioneering the monopole antenna, which has a length of $\lambda/4$ over a corresponding ground plane. Wire antennas are still used today in radio broadcasting, amateur radio, television, and even planar implementations in mobile devices. A $\lambda/2$ dipole has a theoretical feed-point impedance of $73+j42.5\Omega$ [2]. The same length suggests a half-sinusoidal current distribution. There are different methods to calculate the impedance; in this paper, the ratio of electric and magnetic fields at the feed-point gap is considered the input impedance.

The Method of Moments (MoM) is a powerful yet computationally inexpensive numerical technique to solve wave propagation. The Numerical Electromagnetics Code (NEC) was developed in Lawrence Livermore National Labs in the 1970s using MoM to solve wire and surface antennas [3]. Not all antennas have a known theoretical solution. Hence, numerical techniques such as MoM can provide designers with tools to develop new technologies [4].

This paper is divided as follows: Section II presents the derivation for the MoM applied to calculate the surface currents and input impedance of a dipole. Section III shows the resulting input impedance, surface currents, and radiation pattern. Section IV summarizes the results and concludes.

## II. Method Formulation

The Electric Field Integral Equation (EFIE) from the 3D MoM is given by

$$\frac{1}{2}\mathbf{M}_s - \hat{n}\times\mathscr{L}(\bar{\mathbf{J}}_s) + \hat{n}\times\mathscr{K}(\bar{\mathbf{M}}_s) = -\hat{n}\times\mathbf{E}^{inc}(\mathbf{r}) \quad (1)$$

and the Magnetic Field Integral Equation (MFIE) is given by

$$\frac{1}{2}\mathbf{J}_s + \hat{n}\times\mathscr{L}(\bar{\mathbf{M}}_s) + \hat{n}\times\mathscr{K}(\bar{\mathbf{J}}_s) = -\hat{n}\times\mathbf{H}^{inc}(\mathbf{r}) \quad (2)$$

for $\mathbf{r}\in S_o$ in both EFIE and MFIE [5]. $\bar{\mathbf{J}}_s$ and $\bar{\mathbf{M}}_s$ are the electric and magnetic current densities. $\mathscr{L}$ and $\mathscr{L}$ are integral operators over the closed surface $S_o$. $\mathbf{E}^{inc}(\mathbf{r})$ and $\mathbf{H}^{inc}(\mathbf{r})$ are the incident electric and magnetic fields on the surface.

For a thin conducting wire, the transverse fields can be neglected and the total fields can be confined to the longitudinal axis colinear with the wire. The current is assumed to be uniformly distributed along the wire. Under these assumptions and boundary conditions, the EFIE Eq. (1) can be simplified to

$$jk_0Z_0\int_C \hat{l}\cdot\hat{l}'I(\mathbf{r}')G_0(\mathbf{r},\mathbf{r}') + \frac{1}{k_0^2}\frac{dI(\mathbf{r}')}{dl'}\frac{dG_0(\mathbf{r},\mathbf{r}')}{dl}dl' = \hat{l}\cdot\mathbf{E}^{inc}(\mathbf{r}) \quad \mathbf{r}\in C \quad (3)$$

where $C$ denotes the wire path and $\hat{l}$ is the tangential vector. The MoM aims to find the surface current $I(\mathbf{r}')$. The wire is divided into $N$ segments of equal length. The current $I$ is expanded in terms of basis functions, with at least one derivative, between segments given by

$$I(\mathbf{r}') = \sum_{n=1}^{N-1}\Lambda_n(\mathbf{r}')I_n \quad (4)$$

where $\Lambda_n(x')$ is the triangular basis function. $\Lambda_n(x')$ can be defined as

$$\Lambda_n(x') = \begin{cases} \frac{x'-x_{n-1}}{x_n-x_{n-1}}, & \text{if } x_{n-1}\le x'\le x_n \\ = \frac{x_{n+1}-x'}{x_{n+1}-x_n}, & \text{if } x_n\le x'\le x_{n+1}. \end{cases} \quad (5)$$

This basis function ensures that the current at the edges is zero. Substituting the expansion of the current with the basis functions from Eq. (4) into Eq. (3) we obtain the linear system given by

$$jk_0\eta_0\sum_{n=1}^{N-1}I_n\int_C\left[\hat{l}\cdot\hat{l}'\Lambda_n(\mathbf{r}')G_0(\mathbf{r},\mathbf{r}') + \frac{1}{k_0^2}\frac{d\Lambda_n(\mathbf{r}')}{dl'}\frac{dG_0(\mathbf{r},\mathbf{r}')}{dl}\right]dl' = \hat{l}\cdot\mathbf{E}^{inc}(\mathbf{r}), \quad \mathbf{r}\in C. \quad (6)$$

Similarly, the testing functions are applied with the condition of being differentiable at least once in order to transfer the derivative to $G_0(\mathbf{r}, \mathbf{r}')$. By applying Galerkin's formulation and integrating $Z_{mn}$ by parts to reduce the order of the singularity we obtain

$$\sum_{n=1}^{N-1} Z_{mn} I_n = V_m, \quad m = 1, 2, ..., N-1 \tag{7}$$

where

$$Z_{mn} = jk_o Z_0 \int_C \Lambda_m(\mathbf{r}) \hat{l_m} \cdot \int_C \hat{l'_n} \Lambda_n(\mathbf{r}') G_0(\mathbf{r}, \mathbf{r}') dl' dl - \frac{jZ_0}{k_0} \int_C \frac{d\Lambda_m(\mathbf{r})}{dl} \int_C \frac{d\Lambda_n(\mathbf{r}')}{dl'} G_0(\mathbf{r}, \mathbf{r}') dl' dl \tag{8}$$

$$V_m = \int_C \Lambda_m(\mathbf{r}) \hat{l_m} \cdot \mathbf{E^{inc}}(\mathbf{r}) dl. \tag{9}$$

The integral in Eq. (8) can be evaluated effectively with numerical integration when the triangular basis functions do not align. When they align they can be evaluated in two subsegments approximating the basis functions. When the two basis functions overlap, the function has to be evaluated with

$$\Psi = \int_{\Delta l} \int_{\Delta l} G_0(\mathbf{r}, \mathbf{r}') dl' dl = \frac{1}{4\pi} \int_{\Delta l} \int_{\Delta l} \frac{e^{-jk_0 R}}{R} dl' dl \tag{10}$$

where,

$$R = |\mathbf{r} - \mathbf{r}'| = \sqrt{a^2 + (l - l')^2}. \tag{11}$$

The input can be expresed as a voltage potential at the center feedpoint with magnitude $V_0$. The $V_m$ vector will contain the values for the fields and the potential can be directly specified as a constant in the center node. The impedance is obtained from the resulting surface current at the center $I_m$ as

$$Z_{in} = \frac{V_0}{I_m}. \tag{12}$$

This method is called delta-gap source. Note that specifying the potential in PEC is not possible, hence, the center element results will be distorted. The magnetic fill current method avoids this issue by using a current loop around the feed point as the source. Fig. 1 shows the delta-gap source excitation in (a) and the magnetic frill source excitation in (b).

## III. Numerical Experiments

### A. Validation

To validate the numerical results, a $\lambda/2$ dipole for a frequency of 3 GHz was evaluated with a length of $50mm$ and a radius of $0.001\lambda$. Table I shows the input impedances for an increasing number of $\lambda/N$, or $N$ elements per wavelength. Fig. 2 shows the convergence of the real and imaginary components of the feed-point impedance. Note that the real component converges faster than the imaginary component.

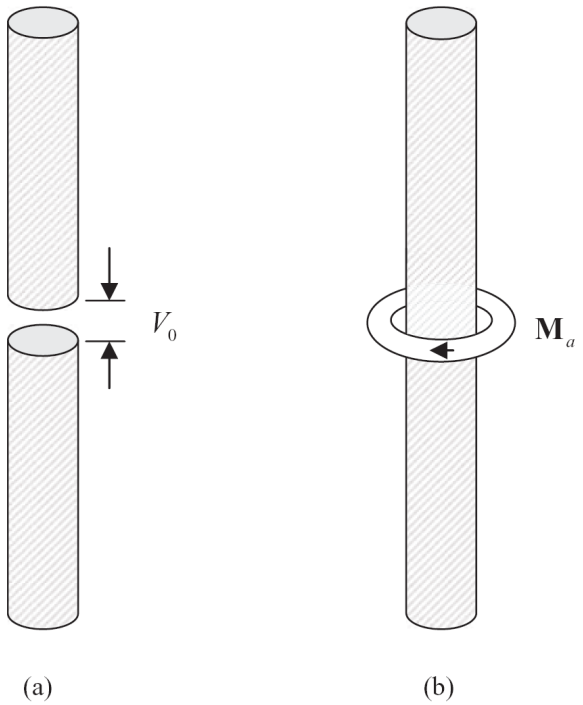


Fig. 1: Wire Antenna Source Feeding Mechanisms

| $\lambda/N$ | $Z_{in}$ |
|---|---|
| 20 | 71.9 - j7.4 |
| 40 | 75.0 + j32.3 |
| 60 | 76.7 + j38.0 |
| 80 | 78.0 + j40.2 |
| 200 | 82.8 + j44.2 |

TABLE I: Input Impedance Numerical Results

Also, at discretizations coarser than $\lambda/20$ the imaginary component is negative. A discretization of $\lambda/60$ is the closest to the theoretical input impedance presented in Section I.

The magnitude of the normalized current distributions for an increasing number of elements per wavelength is shown in Fig. 3. Note that as the number of elements increases, the current is closer to the analytical result of a half-sinusoid. Examining the real and imaginary components more closely in Figs. 4 and 5 note that a finer discretization improves the smoothness of the solution. The imaginary component in Fig. 5 also flips in direction corresponding to the change in input reactance from Fig. 3.

### B. Dipoles

Figs. 6 to 8 show the real and imaginary components of $\lambda/2$, $3\lambda/2$, and $5\lambda/2$ dipoles respectively. These results are obtained with the optimal $\lambda/60$ discretization from Section III-A. Note that at the center feed-point, the imaginary component of the current is not smooth as it slightly drops. This could be attributed to the delta-gap voltage feed-point. Table II shows the input impedance of dipoles with the same dimensions as

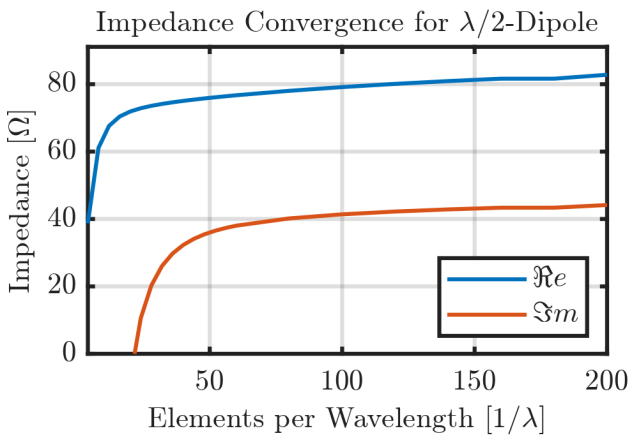


Fig. 2: Input Impedance Convergence

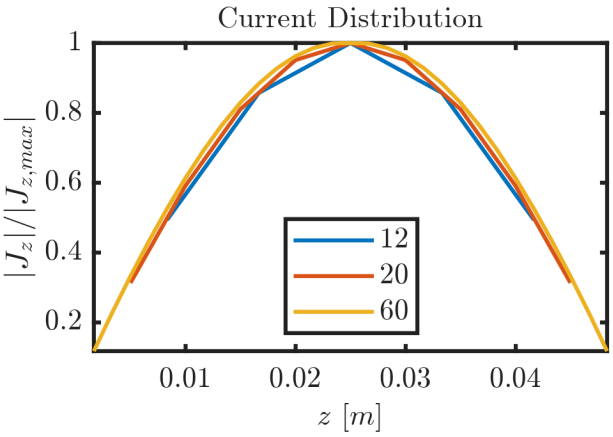


Fig. 3: Current Distribution for different discretizations (elements per $\lambda$)

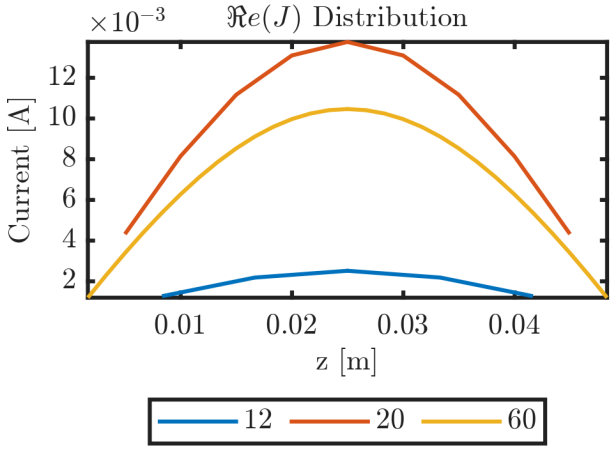


Fig. 4: Real Current Distribution for different discretizations (elements per $\lambda$)

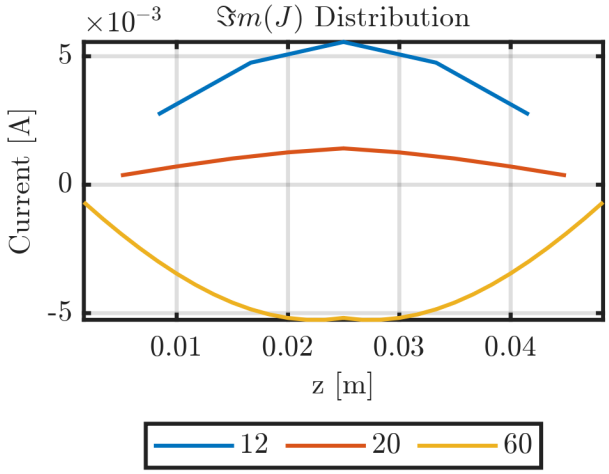


Fig. 5: Reactive Current Distribution for different discretizations (elements per $\lambda$)

| $L$ | $Z_{in}$ |
|---|---|
| $\lambda/2$ | 78.0 + j40.2 |
| $3\lambda/2$ | 110.0 + j38.7 |
| $5\lambda/2$ | 125.9 + j35.9 |

TABLE II: Input Impedance of Dipoles

the previous plots. Note that for longer dipoles, the resistive component increases while the reactive component decreases.

### C. Radiation Pattern

The far-field electric field can be found by adding the contributions for all elements at each observation point with the corresponding phase shift using the following equation [5]

$$E_\theta(r,\theta,\phi) = -\frac{jk_0\eta_0 e^{-jk_0 r}}{4\pi} \iint_{s_p} E_D^{(\theta)} \cdot J_s dS. \qquad (13)$$

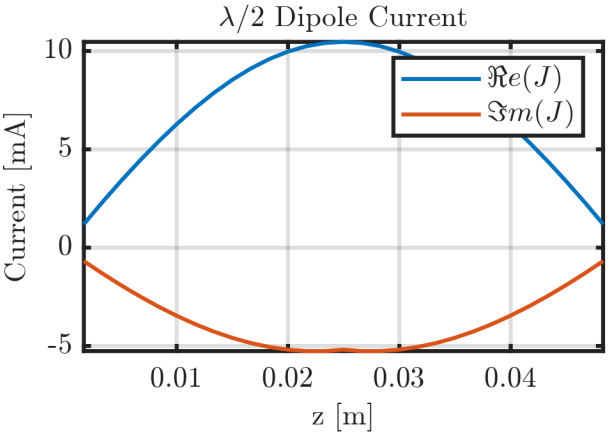


Fig. 6: Current Distribution for $\lambda/2$ Dipole

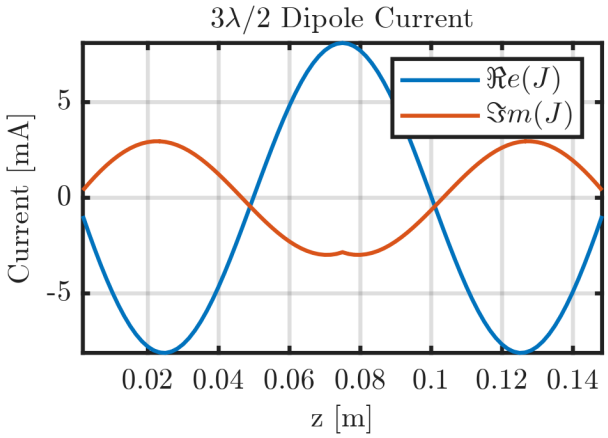


Fig. 7: Current Distribution for $3\lambda/2$ Dipole

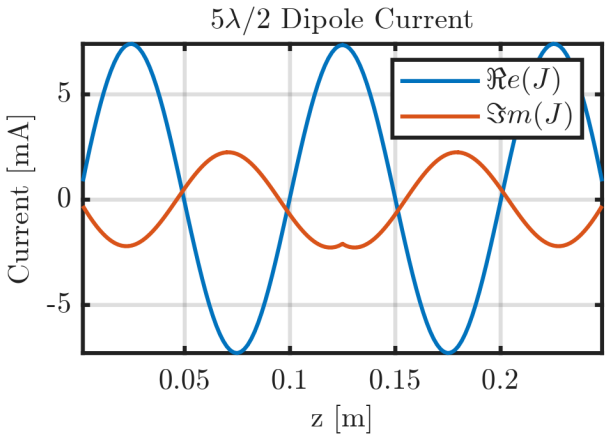


Fig. 8: Current Distribution for $5\lambda/2$ Dipole

The discrete implementation will have the form of

$$E_\theta = -\frac{jk_0\eta_0}{4\pi}\sum_{n=1}^{N-1}\left(\Delta z J(n)\sin(\theta)e^{jk_0 r\cos(\theta)}\right). \quad (14)$$

The radiation patterns corresponding to the dipoles in Section III-B are shown in Fig. 9. Note that as the number of maxima and minima increases, the number of peaks and nulls also increases.

## IV. Conclusion

The Method of Moments is presented and validated with an example of delta-gap center-fed dipoles. The current distribution is analyzed, and the input impedance is calculated from the fields at the feed point. The resulting impedance does not perfectly match the analytical solution. Some plausible causes are the delta-gap feeding technique that creates a discontinuity or the basis and testing functions not providing a proper representation of the field interactions. The radiation pattern is calculated from the surface currents. This code could be improved using a current loop-feeding technique known as magnetic frill current source.

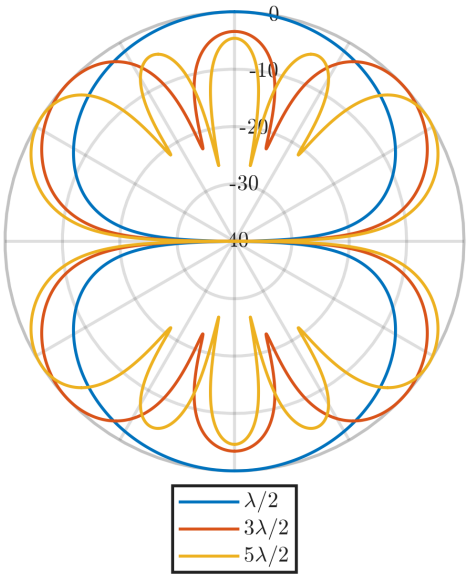


Fig. 9: Radiation Pattern

## References

[1] R. Appleyard, *Pioneers of Electrical Communication*. Essay index reprint series, Books for Libraries Press, 1968.
[2] C. A. Balanis, *Antenna theory: analysis and design*. John wiley & sons, 2016.
[3] "Numerical electromagnics code." Accessed: 2024-04-29.
[4] S. R. Zang and J. R. Bergmann, "Analysis of omnidirectional dual-reflector antenna and feeding horn using method of moments," *IEEE Transactions on Antennas and Propagation*, vol. 62, no. 3, pp. 1534–1538, 2014.
[5] J.-M. Jin, *The Finite Difference Method*, pp. 295–341. Wiley-IEEE Press, 2010.